Magnetic and magnetotransport properties of the orthorhombic perovskites (Lu,Ca)MnO_3

N. Imamura,[1] M. Karppinen,[1,2,*] T. Motohashi,[1] and H. Yamauchi[1]
[1]*Materials and Structures Laboratory, Tokyo Institute of Technology, Yokohama 226-8503, Japan*
[2]*Laboratory of Inorganic Chemistry, Department of Chemistry, Helsinki University of Technology, FI-02015 TKK, Finland*
(Received 19 July 2007; revised manuscript received 25 October 2007; published 22 January 2008)

Here we extend the research of the $(R,Ca)MnO_3$ perovskites to the smallest-R end member $(Lu,Ca)MnO_3$. Magnetic and magnetotransport properties of the $(Lu_{1-x}Ca_x)MnO_3$ system are systematically investigated in regard to carrier doping. It is found that hole doping into the antiferromagnetic $x=0.0$ phase, $LuMnO_3$, causes a spin-glass-like magnetic competition in the wide doping range of $0.1 \leq x \leq 0.6$, whereas electron doping into the antiferromagnetic $x=1.0$ phase, $CaMnO_3$, induces a large magnetoresistance effect for $0.8 \leq x \leq 0.95$.

DOI: 10.1103/PhysRevB.77.024422 PACS number(s): 75.47.Lx, 75.40.Cx, 75.40.Gb, 75.47.Gk

I. INTRODUCTION

The rare-earth (R) manganese oxides, $RMnO_3$, with an orthorhombically distorted perovskite structure have attracted considerable attention because of their various interesting physical properties, including charge ordering, colossal magnetoresistance, and multiferroic characteristics.[1–7] The appearance of such attractive phenomena strongly depends on the degree of carrier doping and accordingly on the mixed valency of manganese, most straightforwardly controlled by means of divalent alkaline-earth (A) substitution at the trivalent R-cation site. In contrast to the multitude of studies on the $(R,A)MnO_3$ systems with the larger R constituents (R=La-Dy), the $(R,A)MnO_3$ perovskite systems with the smaller R constituents (R=Y, Ho-Lu) have remained poorly understood. This is due to the fact that under ordinary synthesis conditions $RMnO_3$ compounds with the smaller Rs adopt a noncentrosymmetric hexagonal structure instead of the perovskite structure.[8,9]

Compared to hexagonal $RMnO_3$, perovskite $RMnO_3$ is denser and should therefore gain stability over the hexagonally structured one under elevated pressures. Indeed, high-pressure (HP) synthesis techniques have been successfully utilized to realize the $RMnO_3$ perovskite phase for the smaller R constituents.[10–13] At the same time, efforts to dope the metastable phases with carriers have been rarely reported and so far focused on limited A-for-R substitution levels.[12,14–18] In the present contribution, magnetic and magnetotransport properties are reported for the $(Lu_{1-x}Ca_x)MnO_3$ system over the whole Ca-for-Lu substitution range, $0.0 \leq x \leq 1.0$.

II. EXPERIMENTAL DETAILS

Single-phase samples of the $(Lu_{1-x}Ca_x)MnO_3$ perovskite were realized over the entire substitution range of $0.0 \leq x \leq 1.0$ employing a variety of synthesis techniques. The phases with $x<0.5$ required a high pressure to form, while the $x \geq 0.5$ phases formed under ambient pressure. The HP synthesis of the lightly Ca-substituted samples was carried out with a cubic-anvil-type HP apparatus at 5 GPa and 1200 °C for 30 min for precursor powders first calcined in air at 900–1300 °C.[12] (Actually for $x=0.0$, single phase $LuMnO_3$ of the hexagonal structure was obtained after air-calcination, which was then converted to the orthorhombic perovskite upon the HP treatment.[12]) The normal-pressure synthesis of heavily Ca-substituted samples was carried out through several heat-treatment periods in air at 1100–1300 °C (each for 12 h) with intermediate grindings. In each case a powder mixture of nominal amounts of Lu_2O_3, $CaCO_3$, and Mn_2O_3 (for $x \leq 0.5$)/MnO_2 (for $x>0.5$) was used as a precursor for the synthesis. However, for both the x ranges the intermediate substitution levels were rather difficult to realize, i.e., $x \approx 0.4$ in the former case and $x=0.7-0.8$ in the latter case. For these compositions, synthesis from a mechanically mixed precursor powder resulted in a mixture of $(Lu_{1-x}Ca_x)MnO_3$ phases with different x values plus traces of impurity phase(s). To enhance the homogeneity of the precursor mixture, a wet chemical route was employed, in which the metal cations dissolved in ~2 M hydrochloric acid were chelated with EDTA (ethylenediaminetetraacetic acid).[19] Through this precursor-preparation route, a single-phase $x=0.8$ sample was obtained.

All the samples were characterized for phase purity and deducing the lattice parameters by x-ray powder diffraction (XRD; Rigaku: RINT2550VK/U equipped with a rotating Cu anode; Cu K_α radiation). Magnetic susceptibility (χ) under a static magnetic field of 0.1 T was measured for the samples from 5 to 400 K using a superconducting quantum interference device (SQUID) magnetometer (Quantum Design: MPMS-XL5). Moreover, ac magnetic susceptibility measurements were carried out with an ac magnetometer (Quantum Design: PPMS 6000) from 5 to 130 K for a frequency range of $10-10^4$ Hz under an ac field of 10 Oe. Electrical resistivity (ρ) measurements were carried out with a four-point-probe method up to 350 K under a dc magnetic field of 0 to 7 T. The dependence of ρ on the strength of external magnetic field (H) was investigated at 5 K under a dc magnetic field of 0 to 7 T.

III. RESULTS

Crystal chemistry. Figure 1 shows XRD patterns for the $(Lu_{1-x}Ca_x)MnO_3$ samples. All the samples were found to be of the pure orthorhombic perovskite phase. The lattice parameters and unit-cell volume were calculated for space group *Pbnm*, and plotted in Fig. 2 with respect to the Ca-substitution level, x. The values obtained for the $x=0.0$, 0.5,

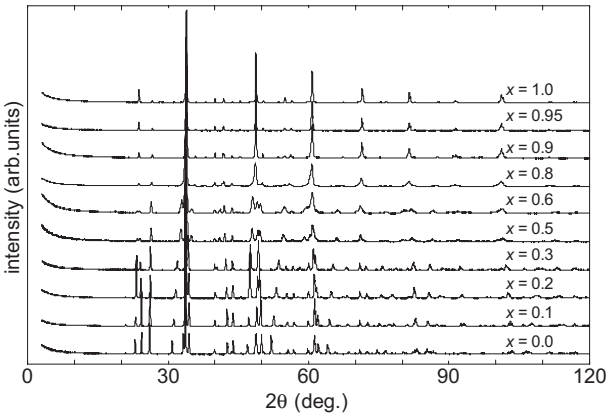

FIG. 1. X-ray powder diffraction patterns for the $(Lu_{1-x}Ca_x)MnO_3$ samples synthesized under various conditions (as described in the text). All samples possess the orthorhombic perovskite structure with space group *Pbnm*. No indication of any impurity phase is seen.

and 1.0 samples are in good agreement with those previously reported for the same compositions.[12,14,20] With increasing x, the lattice parameters change in a continuous manner indicating perfect solid solubility of Ca at the Lu site: Parameters a and c increase slightly, whereas b decreases strongly. As a consequence, the unit-cell volume also decreases. The increases in a and c are explained by the fact that the divalent Ca substituent is larger than the trivalent Lu host cation, whereas the decrease in b (and unit cell volume) is due to the fact that the concentration of the smaller $Mn^{IV}(3d\text{-}t_{2g}^3)$ species increases on the expense of the larger Mn^{III} $(3d\text{-}t_{2g}^3\text{-}e_g^1)$ species. Moreover, the cooperative Jahn-Teller (JT) effect and orbital ordering seen for $RMnO_3$ perovskites[21–24] are

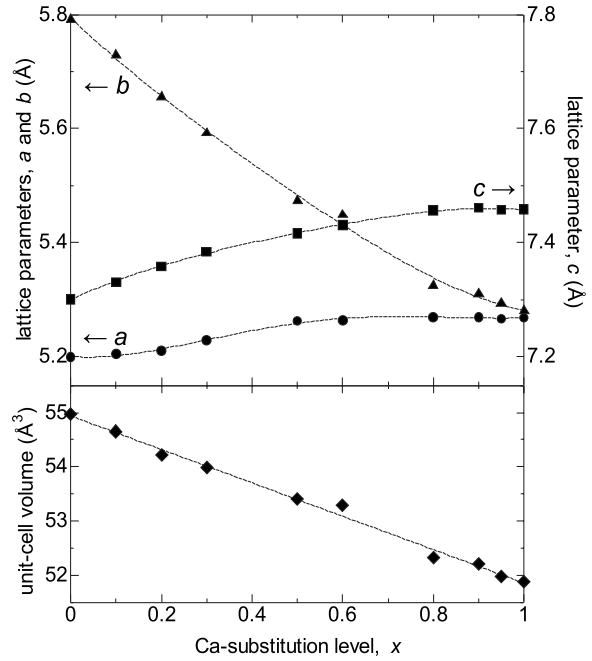

FIG. 2. Lattice parameters, a (•), b (▲), and c (■), and the unit-cell volume (◆) for the $(Lu_{1-x}Ca_x)MnO_3$ samples plotted in terms of the Ca-substitution level, x.

weakened due to the decrease in the concentration of the JT-active e_g electrons.

Magnetic properties. The $\chi-T$ curves registered for the samples in both zero-field-cooled (ZFC) and field-cooled (FC) modes under a static magnetic field of 0.1 T are displayed in Fig. 3. Obviously a variety of magnetic behaviors are seen in the sample series. The $x=0.0$ sample shows a typical antiferromagnetic (AFM) behavior with a cusp in both the ZFC and FC curves about 40 K. With increasing x, the FC $\chi-T$ curves start to deviate from the corresponding ZFC $\chi-T$ curves. For the compositions of $0.1\leq x\leq 0.6$, cusps are seen only for the ZFC $\chi-T$ curves, while the FC magnetizations remain almost constant below the ZFC cusp temperatures (T_g). This implies that the (meta)stable states in the FC and ZFC modes are different below T_g. Such a feature is likely due to spin-glass (SG) states, with freezing temperatures of <30 K for the present samples. The Weiss temperatures (θ) estimated for the samples from the extrapolated $\chi^{-1}-T$ curves are given in Table I: Both negative and positive values are seen for samples located within the expected SG range of $0.1\leq x\leq 0.6$, indicating that AFM and ferromagnetic (FM) couplings are competing with each other when holes are doped into the $(Lu_{1-x}Ca_x)MnO_3$ perovskite phase. Further Ca substitution induces an FM component for $0.8\leq x\leq 0.95$ and eventually, at $x=1.0$, a canted AFM state emerges (Fig. 3).

In order to understand the metastable magnetic states in (Lu,Ca)MnO_3, ac magnetic susceptibility measurements were performed for selected samples at various frequencies (f) varying from 10 to 10^4 Hz with the ac magnetic-field amplitude being fixed at 10 Oe. The data are shown in Fig. 4. Particularly, shown in the upper panel of Fig. 4(a) are the $\chi'-T$ curves for the $x=0.3$ sample that exhibited the largest dc magnetic susceptibility among the samples with the SG-like behavior. A clear cusp is seen at ~27 K, the position of which shifts towards the higher temperature side with increasing f. Such an f-dependent behavior is known to be characteristic to an SG state. On the other hand, the behaviors observed for the $x=0.8$ and 0.9 samples are more complicated; see Figs. 4(b) and 4(c), respectively.

(*Magneto*)*transport properties*. The $\rho-T$ data were recorded for the samples upon decreasing temperature under fixed magnetic fields of 0 and 7 T [Fig. 5(a)]. Metal-like behavior is observed for $x=0.9$, whereas the other samples show insulator or semiconductor behaviors in the absence of the external magnetic field. The ρ values are found to progressively decrease with increasing x up to 0.9 and then again increase for $x>0.9$.

From Fig. 5(a), a significant magnetoresistance (MR) effect is seen for the $x=0.8$, 0.9, and 0.95 samples. The effect is more clearly observed in Fig. 5(b), showing the $\rho-T$ curves of the $x=0.8$ sample as measured under the magnetic fields of 0, 1, 3, 5, and 7 T. The magnitude of the MR effect, on the other hand, is best appreciated from the MR-H data. Figure 6(a) displays the MR $[\equiv(\rho_{7\ T}-\rho_{0\ T})/\rho_{0\ T}]$ ratios determined at 5 K for the $x=0.9$ and 0.95 samples: A large negative MR effect of 50–80 % is seen for the samples. Temperature dependence of the MR effect is shown in Fig. 6(b) for all the three samples exhibiting the MR effect.

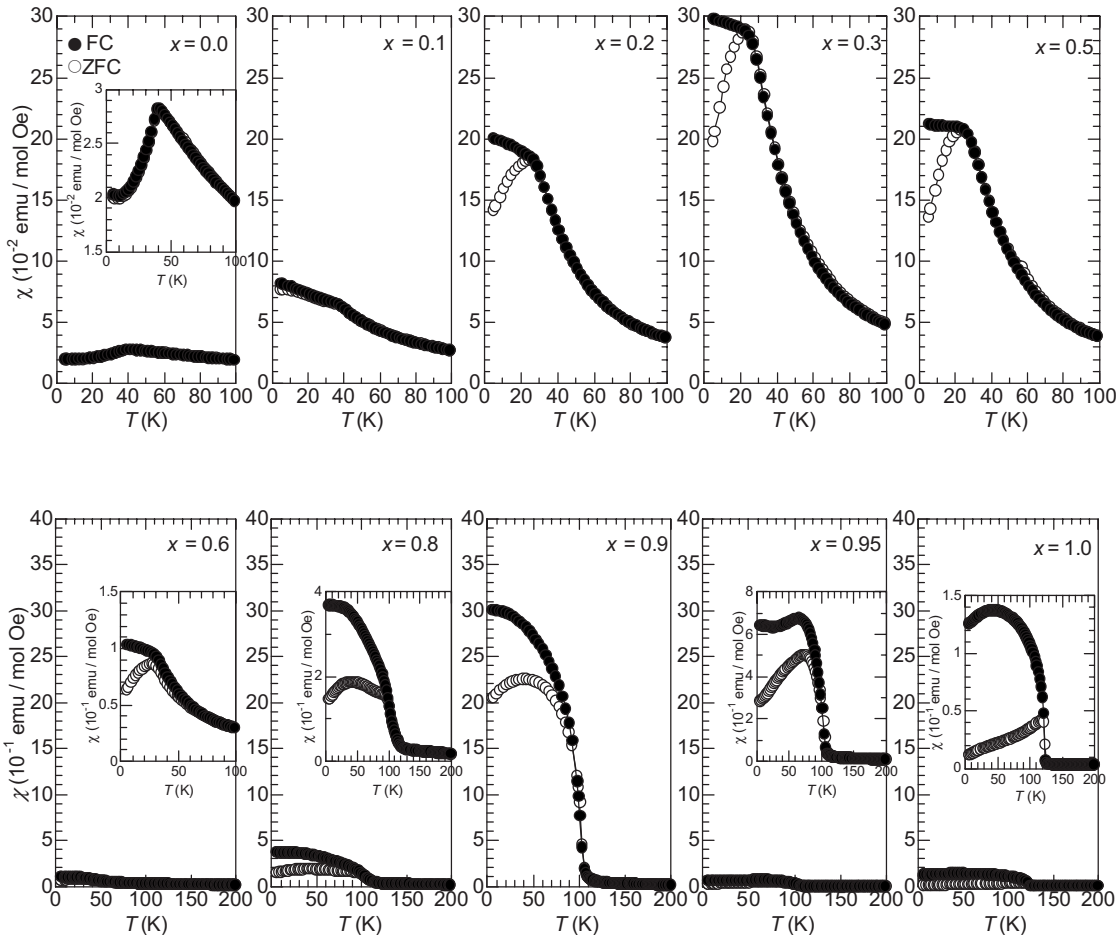

FIG. 3. Temperature (T) dependence of magnetic susceptibility (χ) for the $(Lu_{1-x}Ca_x)MnO_3$ samples measured under an external magnetic field of 0.1 T in both FC and ZFC modes.

IV. DISCUSSION

Composition $x=0.0$. As all the other nondoped $RMnO_3$ perovskites, the parent $LuMnO_3$ phase was found to be an AFM insulator. Accordingly, in the $\chi-T$ curve for the $x=0$ sample a clear cusp was seen about 40 K, in agreement with previous reports.[12,23,24] The AFM ordering was also confirmed from the real part of the ac susceptibility data (not presented here).

TABLE I. Magnetic characteristics of the $(Lu_{1-x}Ca_x)MnO_3$ samples.

x	T_N, T_C, or T_g	θ
0.0	40	−105
0.1	37	−59
0.2	25	−41
0.3	24	31
0.5	24	38
0.6	28	32
0.8	109	86
0.9	104	67
0.95	105	33
1.0	124	−436

Compositions $0.1\leq x\leq 0.6$. For the hole-doped $(R,Ca)MnO_3$ systems, a variety of magnetic and transport properties have been observed with decreasing size of R, i.e., FM metallic state, FM insulating state and SG insulating state for R=La,[25] Pr,[26,27] Sm,[27] and Y,[15–18] respectively. In other words, with decreasing size of the R constituent the FM state gradually gets disfavored. The observed magnetic and transport characteristics of the present $(Lu,Ca)MnO_3$ system resemble those of R=Y,[15–18] such that within the Ca-substitution range of $0.1\leq x\leq 0.6$ the $(Lu_{1-x}Ca_x)MnO_3$ samples seem to be SG insulators with freezing temperatures of <30 K.

The SG state is commonly verified from ac magnetic susceptibility data [measured at various frequencies, f; see Fig. 4(a) for $x=0.3$], employing the quantity K defined by[28]

$$K = 2.3\Delta(\log T_g)/\Delta(\log f), \tag{1}$$

where T_g is the cusp temperature of the $\chi'-T$ curve, and Δ refers to the difference between measurements at two different frequencies which were set at 10 Hz and 10^4 Hz in the present work. For a typical SG system, K is found to be between 0.005–0.08 while $K>0.1$ for a superparamagnet.[28] For the present $x=0.3$ sample, K was determined at 0.009 in accordance with the suggested SG state.

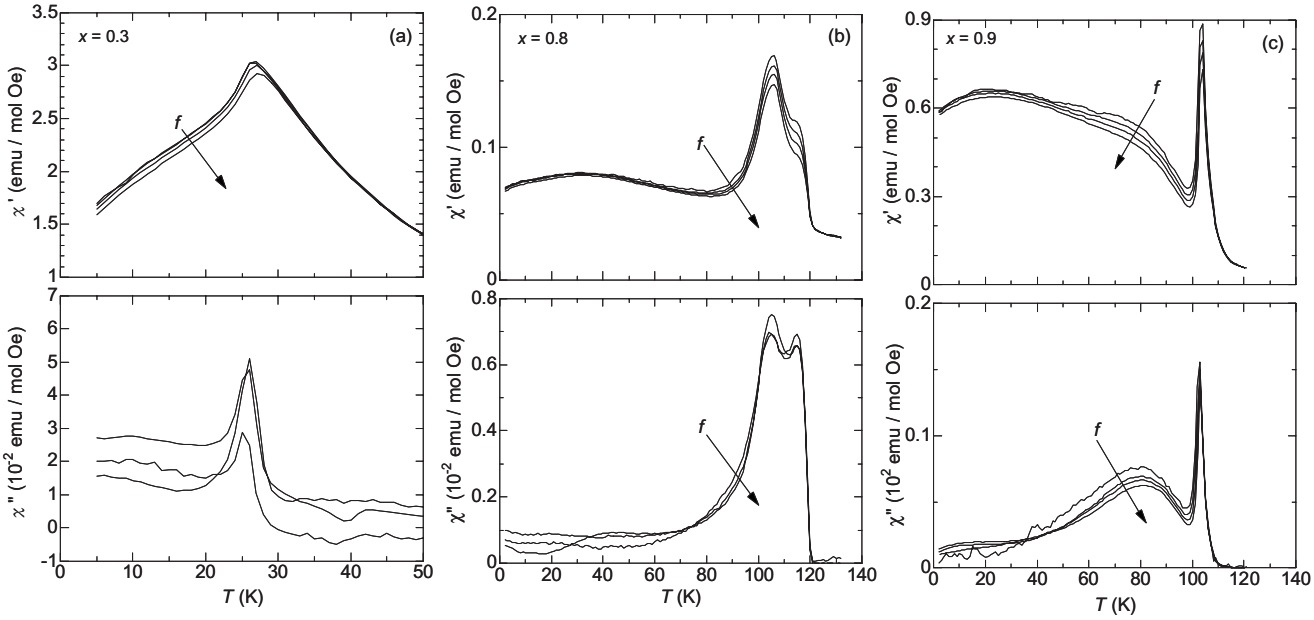

FIG. 4. Real part $\chi'-T$ (upper panel) and imaginary part $\chi''-T$ (lower panel) of the ac magnetic susceptibility for the (a) $x=0.3$, (b) $x=0.8$, and (c) $x=0.9$ samples. The magnitude of the ac field was 10 Oe and the frequency (f) varied as 10 Hz, 10^2 Hz, 10^3 Hz, and 10^4 Hz.

To look more deeply into the ac susceptibility versus temperature data on approaching the T_g from the higher temperature side, we assume a critical slowing-down phenomenon for the spin system near T_{SG} and employ the following expression for the dependence of the maximum relaxation time on T_g.[28–30]

$$\tau_{max} = \tau_0[(T_g - T_{SG})/T_{SG}]^{-z\nu}, \tag{2}$$

where $\tau_{max}=(2\pi f)^{-1}$ (the relaxation time at T_g), τ_0 is a microscopic relaxation time, T_{SG} approaches T_g as $f\rightarrow 0$, and $z\nu$ is a critical exponent. As shown in Fig. 7, the data for $x=0.3$ can well be fitted to the relation described by Eq. (2) if $T_{SG}=26.4$ K is employed (see below for the determination of this value). For various SG materials, $z\nu$ varies typically from 4 to 12.[28] Here, for the $x=0.3$ sample, we estimate the $z\nu$ value at 5.1. At the same time a least-square fitting to the raw T_g versus f data yielded the other two parameters, $\tau_0=7.1\times10^{-13}$ s and $T_{SG}=26.4$ K, which are physically reasonable. Hence we may conclude that the ac susceptibility data agree with the SG hypothesis.

In $(R_{1-x}A_x)MnO_3$ perovskites, the size mismatch (σ^2) between the two cations, R^{III} and A^{II}, that occupy the same cation site is commonly expressed as[31]

$$\sigma^2 \equiv xr_A^2 + (1-x)r_R^2 - 2[xr_A + (1-x)r_R]^2, \tag{3}$$

where $r_A(r_R)$ is the ionic radius of A^{II} (R^{III}). The magnitude of σ^2 is believed to correlate with the appearance of the SG insulator state such that the larger the σ^2 value is the more favored the SG insulator state is.[32,33] Our finding of a SG insulator state for $(Lu_{0.7}Ca_{0.3})MnO_3$ is in agreement with its large σ^2 value of 4.29×10^{-3} Å^2, which is much larger than that of $(Dy_{0.7}Ca_{0.3})MnO_3$ (1.82×10^{-3} Å^2) without a cusp in its $\chi'-T$ curve.[33] We thus conclude that the local structural changes induced by the large size mismatch between the cations, Lu^{III} and Ca^{II}, and the strongly distorted crystal structure most likely cause the magnetic competition in $(Lu,Ca)MnO_3$.

Finally, we note that the $\rho-T$ data [Fig. 5(a)] is in accordance with the SG insulator scheme for $0.1\leq x\leq 0.6$, showing insulating behaviors for all the samples in this x range. Apparently as the size of R decreases, the double exchange (DE) mechanism[34,35] does not work anymore, i.e., the hopping of doped holes is constrained by the enhanced tilting of the MnO_6 octahedral network. It should also be noted that the magnitude of resistivity was found to progressively decrease with increasing Ca content [Fig. 5(a)]. As for the $x=0.5$ sample, neither the $\rho-T$ nor the $\chi-T$ curve yielded any indication of the charge ordering phenomenon commonly seen for the $(R_{0.5}Ca_{0.5})MnO_3$ perovskites with the larger R constituents.[14] This is in accordance with the results of previous work on $(Lu_{0.5}Ca_{0.5})MnO_3$.[12,14]

Compositions $0.8\leq x\leq 0.95$. For the heavily Ca-substituted $(Lu_{1-x}Ca_x)MnO_3$ samples of $0.8\leq x\leq 0.95$, an FM component was clearly observed in the $\chi-T$ data (Fig. 3). Also the Weiss temperatures were positive (Table I). The appearance of an FM state in the Ca-rich region, i.e., in the electron-doped range in the vicinity of $CaMnO_3$, is a feature seen for all the $(R_{1-x}Ca_x)MnO_3$ perovskite systems independent of the species of R.[36–39] The $\chi''-T$ curves shown in Figs. 4(b) and 4(c) for $x=0.8$ and 0.9 clearly exhibit a sharp maximum (at ~115 and ~103 K, respectively) that can be assigned to the FM transition. The T_C values determined from the $\chi''-T$ curves are in good agreement with those estimated for the same samples from the dc magnetic susceptibility curves, $\chi-T$. For the $x=0.8$ sample another anomaly is seen at 106 K in Fig. 4(b), which is close to the separation temperature of the FC and ZFC magnetizations in this sample. Based on the phase diagram reported in Ref. 39 for the C-type (with charge ordering) and G-type (canted) AFM

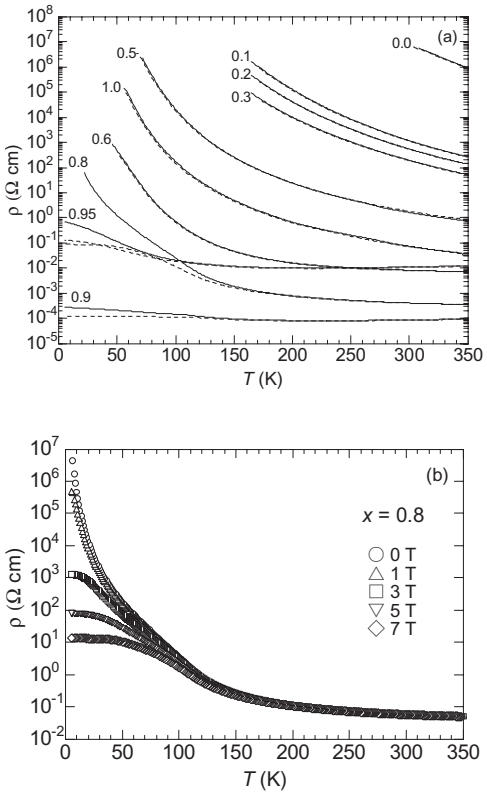

FIG. 5. Temperature (T) dependence of electrical resistivity (ρ) measured (a) for the various $(Lu_{1-x}Ca_x)MnO_3$ samples under an external magnetic field of 0 T (solid lines) and 7 T (dotted lines), and (b) for the $x=0.8$ sample under various external magnetic fields.

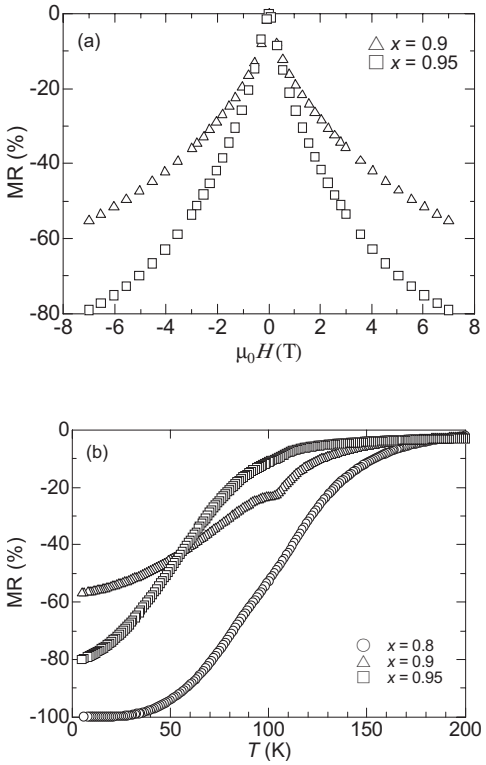

FIG. 6. (a) Field (H) dependence of the MR ratio for the $x=0.9$ and 0.95 samples measured at 5 K, and (b) the temperature (T) dependence of the MR ratio for the $x=0.8$, 0.9, and 0.95 samples.

phases in terms of x in $(R_{1-x}Ca_x)MnO_3$, the present $x=0.8$ sample of $(Lu_{0.2}Ca_{0.8})MnO_3$ would be located at the very boundary between the two phases, like $(Pr_{0.125}Ca_{0.875})MnO_3$ that was suggested to have a two-phase structure.[39] Also the large difference between the FC and ZFC magnetizations is a feature common for $(Pr_{0.125}Ca_{0.875})MnO_3$[39] and the present $x=0.8$ sample (Fig. 3). Hence it is possible that at $x=0.8$ the $(Lu_{1-x}Ca_x)MnO_3$ system too could have the two-phase structure and accordingly the lower-temperature peak seen in the $\chi''-T$ curve for this sample might be due to the charge ordering accompanied by the C-type AFM order. In other words, the lower- and higher-temperature peaks in the ac magnetization data directly correspond to the point of segregation between FC and ZFC and the onset of magnetization in the dc magnetization data, respectively.

It is believed that also the average size of the R^{III} and A^{II} cations influences the magnetic characteristics in the electron-doped region such that the stability of the FM metallic state gets wider for the smaller R constituents.[36] Also the size-mismatch between the two cation species affects the magnetic property.[36] For high x values, the situation is considered such that electrons are doped into the canted AFM $CaMnO_3$ matrix. Detailed investigations of La-[40–42] and Sm-substituted[43] $CaMnO_3$ have revealed a magnetic phase separation such that FM clusters may exist randomly in an AFM matrix. The R^{III}/Ca^{II} size-mismatch is larger in the present (Lu,Ca)MnO_3 system than in the other (R,Ca)MnO_3 systems. This could make the doped carriers more localized and result in a complex magnetism.

As discussed above, the dc magnetization characteristics for the $x\geq 0.8$ samples of the $(Lu_{1-x}Ca_x)MnO_3$ system are parallel to those of the other (R,Ca)MnO_3 systems, even though in the lower substitution range ($0.1\leq x\leq 0.6$) the Lu-based system presents a wide glassy state that is not seen for the (R,Ca)MnO_3 systems of the larger R constituents. Moreover, careful inspection of the evolution of lattice parameters with increasing x (Fig. 2) reveals that the changes are less pronounced for the heavily Ca-substituted samples compared with the lightly Ca-substituted samples. In the case of $x=0.9$, for instance, the $\chi-T$ and $\rho-T$ curves together with the

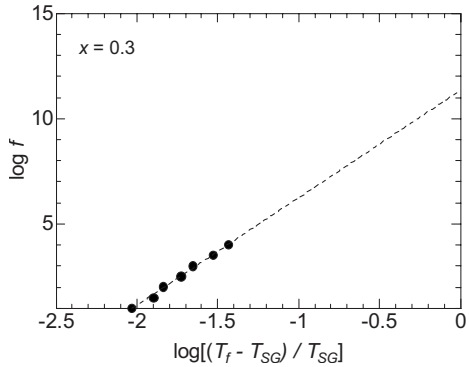

FIG. 7. $\log f$ vs $\log[(T_g-T_{SG})/T_{SG}]^{-z\nu}$ plots for the $x=0.3$ sample. Three parameters (τ, T_{SG}, and $z\nu$) are estimated from the presented dotted line, which is drawn best on the standard theory for dynamical scaling near a phase transition (shown in the text).

$\chi''-T$ curve (which displays an FM transition and a broad maximum at lower temperatures) closely resemble those of the cluster-glass compounds.[44,45] That is, the FM transition emerges first and then a frequency-dependent behavior is seen at the lower temperatures. The bump at a low temperature (around 80 K in $\chi''-T$) is almost identical to that reported for $(Sm_{0.1}Ca_{0.9})MnO_3$,[44] suggesting that $(Lu_{0.1}Ca_{0.9})MnO_3$ may also have a cluster-glass metallic state.

A significant magnetoresistance (MR) effect was seen for the $x=0.8$, 0.9, and 0.95 samples. The magnetotransport properties revealed for the present $(Lu,Ca)MnO_3$ perovskites are exactly what one could expect on the bases of the trend previously seen for the $(R,Ca)MnO_3$ system as the size of the R constituent decreases.[36,38] The origin of this phenomenon, e.g., whether it is an intrinsic property or attributable to grain boundaries, cannot be determined on the bases of the present data for polycrystalline samples. However, as seen in Fig. 5(b), larger external magnetic field induces an insulator-metal transition to give a large negative MR effect. Such a phenomenon can not be explained by a grain-boundary effect only, and accordingly it seems reasonable to consider that the MR effect has as an intrinsic character. In other words, that the FM component is enhanced by the application of an external magnetic field assists the wide-range DE-like electron hopping between parallel Mn^{IV} spin sites. Here we acknowledge the importance of a detailed structural investigation by means of, e.g., neutron powder diffraction.

Composition $x=1.0$. For the $x=1.0$ sample, a weak FM was observed in accordance with the previously reported magnetization results for $CaMnO_3$.[44,46] The large negative Weiss temperature supports canted AFM in the sample. Insulating behavior seen in the $\rho-T$ curve also agrees with the previous reports for $CaMnO_3$.[39,44]

V. CONCLUSIONS

The $(Lu,Ca)MnO_3$ perovskite system was systematically investigated for the magnetic and magnetotransport properties in regards to the carrier-doping level. For most of the compositions an insulator or a semiconductor behavior was seen (under zero external magnetic field), but the $x=0.9$ sample showed metal-like behavior. Like the other nondoped $RMnO_3$ phases, $LuMnO_3$ showed an AFM behavior. Upon doping the phase with holes, an SG-like behavior emerged in the wide range of $0.1 \leq x \leq 0.6$ as a consequence of the strongly distorted crystal structure and the large Lu/Ca size mismatch. On the other hand, the Ca-rich samples with $0.8 \leq x < 1.0$ were found to exhibit an FM behavior and a large negative MR effect.

Comparison of the present $(Lu_{1-x}Ca_x)MnO_3$ system to the other $(R_{1-x}Ca_x)MnO_3$ systems revealed that within the doping range of $0.1 \leq x \leq 0.6$ it resembles the $(R_{1-x}Ca_x)MnO_3$ systems with the smaller R constituents only, e.g., $(Y_{1-x}Ca_x)MnO_3$, whereas in the doping range of $0.8 \leq x \leq 0.95$ all the $(R_{1-x}Ca_x)MnO_3$ systems are essentially alike. In other words, for the low Ca-substitution levels the magnetic and (magneto)transport properties of the $(R,Ca)MnO_3$ perovskites significantly depend on the size of the R cation, whereas for the high substitution levels, the properties are less affected by the choice of R.

ACKNOWLEDGMENTS

This work was supported by Grants-in-Aid for Scientific Research (No. 15206002) from the Japan Society for the Promotion of Science, Academy of Finland (Decision Nos. 114517 and 116254), and also by MSL's International Collaborative Research Project-2007 (Tokyo Tech).

*Corresponding author. Laboratory of Inorganic Chemistry, Department of Chemistry, Helsinki University of Technology, P.O. Box 6100, FI-02015 TKK, Finland. FAX: +358-9-462 373. maarit.karppinen@tkk.fi

[1] J. Volger, Physica (Amsterdam) **20**, 49 (1954).
[2] R. von Helmolt, J. Wecker, B. Holzapfel, L. Schultz, and K. Samwer, Phys. Rev. Lett. **71**, 2331 (1993).
[3] H. Y. Hwang, S.-W. Cheong, P. G. Radaelli, M. Marezio, and B. Batlogg, Phys. Rev. Lett. **75**, 914 (1995).
[4] Z. J. Huang, Y. Cao, Y. Y. Sun, Y. Y. Xue, and C. W. Chu, Phys. Rev. B **56**, 2623 (1997).
[5] M. Fiebig, Th. Lottermoser, D. Fröhlich, A. V. Goltsev, and R. V. Pisarev, Nature (London) **419**, 818 (2002).
[6] T. Kimura, T. Goto, H. Shintani, K. Ishizaka, T. Arima, and Y. Tokura, Nature (London) **426**, 55 (2003).
[7] Y. Tomioka, A. Asamitsu, Y. Moritomo, H. Kuwahara, and Y. Tokura, Phys. Rev. Lett. **74**, 5108 (1995).
[8] H. L. Yakel, Acta Crystallogr. **8**, 394 (1955).
[9] H. L. Yakel, W. C. Koehler, E. F. Bertaut, and E. F. Forrat, Acta Crystallogr. **16**, 957 (1963).
[10] A. Waintal, J. Capponi, E. F. Bertaut, M. Contré, and D. Francois, Solid State Commun. **4**, 125 (1966); A. Waintal and J. Chevanas, Mater. Res. Bull. **2**, 819 (1967).
[11] Y. H. Huang, H. Fjellvåg, M. Karppinen, B. C. Hauback, H. Yamauchi, and J. B. Goodenough, Chem. Mater. **18**, 2130 (2006); **19**, 2139 (2007).
[12] N. Imamura, M. Karppinen, H. Fjellvåg, and H. Yamauchi, Solid State Commun. **140**, 386 (2006).
[13] K. Uusi-Esko, J. Malm, N. Imamura, H. Yamauchi, and M. Karppinen (unpublished).
[14] K. Yoshii and H. Abe, J. Solid State Chem. **165**, 131 (2002); K. Yoshii, H. Abe, and N. Ikeda, *ibid.* **178**, 3615 (2005).
[15] X. L. Wang, J. Horvat, H. K. Liu, and S. X. Dou, J. Magn. Magn. Mater. **182**, L1 (1998).
[16] R. Mathieu, P. Nordblad, D. N. H. Nam, N. X. Phuc, and N. V. Khiem, Phys. Rev. B **63**, 174405 (2001).
[17] D. Sedmidubský, J. Hejtmánek, M. Maryško, Z. Jirák, V. Hardy, and C. Martin, J. Appl. Phys. **91**, 8260 (2002).
[18] M. Dlouhá, S. Vratislav, Z. Jirák, J. Hejtmánek, K. Knížek, and D. Sedmidubský, Appl. Phys. A: Mater. Sci. Process. **74**, S673 (2002).
[19] Y. H. Huang, J. Lindén, H. Yamauchi, and M. Karppinen, Chem.

Mater. **16**, 4337 (2004).
[20] Q. Zhou and B. J. Kennedy, J. Phys. Chem. Solids **67**, 1595 (2006).
[21] H. W. Brinks, H. Fjellvåg, and A. Kjekshus, J. Solid State Chem. **129**, 334 (1997); H. W. Brinks, J. Rodriguez-Carvajal, H. Fjellvåg, A. Kjekshus, and B. C. Hauback, Phys. Rev. B **63**, 094411 (2001).
[22] J. A. Alonso, M. J. Martínez-Lope, M. T. Casais, and M. T. Fernández-Díaz, Inorg. Chem. **39**, 917 (2000).
[23] J.-S. Zhou, J. B. Goodenough, J. M. Gallardo-Amores, E. Morán, M. A. Alario-Franco, and R. Caudillo, Phys. Rev. B **74**, 014422 (2006).
[24] M. Tachibana, T. Shimoyama, H. Kawaji, T. Atake, and E. Takayama-Muromachi, Phys. Rev. B **75**, 144425 (2007).
[25] P. Schiffer, A. P. Ramirez, W. Bao, and S.-W. Cheong, Phys. Rev. Lett. **75**, 3336 (1995).
[26] Y. Tomioka, A. Asamitsu, H. Kuwahara, Y. Moritomo, and Y. Tokura, Phys. Rev. B **53**, R1689 (1996).
[27] C. Martin, A. Maignan, M. Hervieu, and B. Raveau, Phys. Rev. B **60**, 12191 (1999).
[28] See, for example, J. A. Mydosh, *Spin Glasses* (Taylor & Francis, London, 1993).
[29] P. C. Hohenberg and B. I. Halperin, Rev. Mod. Phys. **49**, 435 (1977).
[30] K. Gunnarsson, P. Svedlindh, P. Nordblad, L. Lundgren, H. Aruga, and A. Ito, Phys. Rev. Lett. **61**, 754 (1988).
[31] L. M. Rodriguez-Martinez and J. P. Attfield, Phys. Rev. B **54**, R15622 (1996).
[32] T. Terai, T. Kakeshita, T. Fukuda, T. Saburi, N. Takamoto, K. Kindo, and M. Honda, Phys. Rev. B **58**, 14908 (1998).
[33] A. Maignan, C. Martin, G. Van Tendeloo, M. Hervieu, and B. Raveau, Phys. Rev. B **60**, 15214 (1999).
[34] C. Zener, Phys. Rev. **82**, 403 (1951).
[35] P. G. de Gennes, Phys. Rev. **118**, 141 (1960).
[36] B. Raveau, A. Maignan, C. Martin, and M. Hervieu, Chem. Mater. **10**, 2641 (1998); B. Raveau, A. Maignan, C. Martin, and M. Hervieu, J. Supercond. **12**, 1 (1999).
[37] A. Maignan, C. Martin, F. Damay, and B. Raveau, Chem. Mater. **10**, 950 (1998).
[38] B. Raveau, M. Hervieu, A. Maignan, and C. Martin, J. Mater. Chem. **11**, 29 (2001).
[39] H. Fujishiro, M. Ikebe, S. Ohshiden, and K. Noto, J. Phys. Soc. Jpn. **69**, 1865 (2000).
[40] J. J. Neumeier and J. L. Cohn, Phys. Rev. B **61**, 14319 (2000).
[41] C. D. Ling, E. Granado, J. J. Neumeier, J. W. Lynn, and D. N. Argyriou, Phys. Rev. B **68**, 134439 (2003).
[42] E. Granado, C. D. Ling, J. J. Neumeier, J. W. Lynn, and D. N. Argyriou, Phys. Rev. B **68**, 134440 (2003).
[43] C. Martin, A. Maignan, M. Hervieu, B. Raveau, Z. Jirák, M. M. Savosta, A. Kurbakov, V. Trounov, G. André, and F. Bourée, Phys. Rev. B **62**, 6442 (2000).
[44] A. Maignan, C. Martin, F. Damay, B. Raveau, and J. Hejtmanek, Phys. Rev. B **58**, 2758 (1998).
[45] D. N. H. Nam, K. Jonason, P. Nordblad, N. V. Khiem, and N. X. Phuc, Phys. Rev. B **59**, 4189 (1999).
[46] J. B. MacChesney, H. J. Williams, J. F. Potter, and R. C. Sherwood, Phys. Rev. **164**, 779 (1967).